Received: 25 November 2021 | Revised: 13 January 2022 | Accepted: 31 January 2022

DOI: 10.1002/hbm.25808

RESEARCH ARTICLE

WILEY

Disrupted topological organization of resting-state functional brain networks in cerebral small vessel disease

Haotian Xin[1] | Hongwei Wen[2,3] | Mengmeng Feng[1] | Yian Gao[4] | Chaofan Sui[4] | Nan Zhang[4] | Changhu Liang[4] | Lingfei Guo[4]

[1]Department of Radiology, Shandong Provincial Hospital, Cheeloo College of Medicine, Shandong University, Jinan, Shandong, China

[2]Key Laboratory of Cognition and Personality (Ministry of Education), Chongqing, China

[3]School of Psychology, Southwest University, Chongqing, China

[4]Department of Radiology, Shandong Provincial Hospital Affiliated to Shandong First Medical University, Jinan, Shandong, China

Correspondence
Lingfei Guo, Department of Radiology, Shandong Provincial Hospital Affiliated to Shandong First Medical University, 324 Jingwu Road, Jinan, Shandong 250021, China.
Email: glfsci@163.com

Abstract

We aimed to investigate alterations in functional brain networks and assess the relationship between functional impairment and topological network changes in cerebral small vessel disease (CSVD) patients with and without cerebral microbleeds (CMBs). We constructed individual whole-brain, region of interest (ROI) level functional connectivity (FC) networks for 24 CSVD patients with CMBs (CSVD-c), 42 CSVD patients without CMBs (CSVD-n), and 36 healthy controls (HCs). Then, we used graph theory analysis to investigate the global and nodal topological disruptions between groups and relate network topological alterations to clinical parameters. We found that both the CSVD and control groups showed efficient small-world organization in FC networks. However, compared to CSVD-n patients and controls, CSVD-c patients exhibited a significantly decreased clustering coefficient, global efficiency, and local efficiency and an increased shortest path length, indicating a disrupted balance between local specialization and global integration in FC networks. Although both the CSVD and control groups showed highly similar hub distributions, the CSVD-c group exhibited significantly altered nodal betweenness centrality (BC), mainly distributed in the default mode network (DMN), attention, and visual functional areas. There were almost no global or regional alterations between CSVD-n patients and controls. Furthermore, the altered nodal BC of the right anterior/posterior cingulate gyrus and left cuneus were significantly correlated with cognitive parameters in CSVD patients. These results suggest that CSVD patients with and without CMBs had segregated disruptions in the topological organization of the intrinsic functional brain network. This study advances our current understanding of the pathophysiological mechanisms underlying CSVD.

KEYWORDS
cerebral microbleeds, cerebral small vessel disease, functional connectivity, graph theory, topological organization

Haotian Xin and Hongwei Wen contributed equally and share the first authorship.

Lingfei Guo and Changhu Liang contributed equally and share the corresponding author.

1 | INTRODUCTION

Cerebral small vessel disease (CSVD) is a common disease that seriously endangers public health. It refers to a series of clinical, imaging, and pathological syndromes caused by various etiologies affecting the cerebral arteries, arterioles, venules, and capillaries (Pantoni, 2010). CSVD plays a crucial role in various conditions, including stroke, dementia, and aging (Miwa et al., 2014; Thompson & Hakim, 2009). Based on a clinical survey, the proportion of dementia caused by CSVD is as high as 36% to 67% in this decade (Grau-Olivares & Arboix, 2009), leading to cognitive decline and functional loss in the elderly (O'Brien et al., 2003). Imaging markers of CSVD include recent small subcortical infarcts, lacunes, white matter hyperintensities (WMHs), perivascular spaces, cerebral microbleeds (CMBs), and brain atrophy, and these lesions may exist individually or in various combinations (Wardlaw et al., 2013).

With the development of neuroimaging technology, CMBs have been widely studied. CMBs can be detected using T2*-weighted gradient-recalled echo (GRE) or susceptibility-weighted imaging (SWI) sequences, and are visible as small round or ovoid areas of hypointense lesions that range in diameter between 2 and 5 mm and correspond to perivascular collections of hemosiderin deposits (Cordonnier, 2011). Hypertensive vasculopathy and cerebral amyloid angiopathy are two main types of vascular pathology that cause CMBs (Greenberg et al., 2009). Numerous epidemiological studies have illustrated that CMBs have a significant impact on overall cognitive function, executive function, and information processing speed (Nannoni et al., 2021; van Es et al., 2011; Werring et al., 2004). Furthermore, Stefania Nannoni et al. suggested that CMBs were independently associated with cognitive impairment (CI). In elderly patients without dementia, CMBs in the frontal and temporal lobes are related to cognitive ability, independent of other small vascular disease-related lesions (van Norden et al., 2011). CMBs can affect the cognitive performance of CSVDs. According to the simple SVD score and amended score (Amin Al Olama et al., 2020), the presence of CMBs can directly raise the CSVD score. CMBs can be used as a biological marker of cerebral microangiopathy (Seo et al., 2007). Moreover, the occurrence of CMBs is correlated with the risk of recurrent cerebral hemorrhage, which indicates that CMBs play an important role in the diagnosis of cerebral amyloidosis and evaluation of prognosis of this disease (Samarasekera, Smith, & Al-Shahi Salman, 2012). However, the neurobiological mechanism by which CMBs lead to CI in CVSD patients remains unclear. Therefore, it is of great clinical significance to further study this relationship and provide theoretical support for effective prevention and treatment.

Recently, noninvasive resting-state functional MRI (rs-fMRI) has emerged as a promising imaging modality for CSVD studies. rs-fMRI depends on spontaneous low-frequency fluctuations in the blood oxygenation level-dependent (BOLD) signal (Damoiseaux et al., 2006). Existing rs-fMRI studies have exhibited altered amplitudes of low-frequency fluctuations (ALFFs) (Yi et al., 2012) and regional homogeneity (ReHo) (Ding et al., 2017) in CSVD patients. And more recent studies have implemented a network science approach to measure FC. For instance, Sun et al. (2011) first reported altered FC between the posterior cingulate gyrus (PCG) and the temporal and frontal regions in CSVD patients with CI. Additionally, in a combined analysis of CSVD patients with and without CI, the authors demonstrated decreased within-network function of the default mode network (DMN) and lower negative connectivity between the DMN and other networks, including the dorsal attention network (DAN) and the frontoparietal control network (FPCN), in CSVD patients (Liu et al., 2019). However, these studies have two main drawbacks. First, the two first measures could not directly characterize pairwise correlations between brain regions. Second, as an interconnected network, the human brain continuously integrates information across numerous brain regions, displaying various crucial topological properties (Wang et al., 2013). The latter two studies revealed functional changes only in a few specific and local networks or circuits.

In recent years, graph theory analysis has become increasingly popular in the neuroimaging and brain network analysis fields, providing advanced tools to investigate the topological organization of brain networks, which may offer important insights that can unravel the underlying mechanisms of CSVD. Different from seed-based analysis, which focuses merely on the strength of correlation between one ROI and another, graph theory measures the topological properties of ROIs across the entire brain or networks associated with specific functions (Kana, Uddin, Kenet, Chugani, & Müller, 2014), thereby constructing a powerful framework for describing the topological architecture and potential disruptions of the brain connectome (Zhu et al., 2020). In particular, graph theory analysis revealed that FC networks exhibit many crucial topological properties, such as small worldness and highly connected hubs (Wen et al., 2018). Graph theory analysis has been widely used to reveal cortical FC and research the pathophysiological changes in psychiatric and neurologic disorders, such as Alzheimer disease (He, Chen, Gong, & Evans, 2009), Parkinson disease (Qiu et al., 2021), schizophrenia (van den Heuvel & Fornito, 2014; Zhu et al., 2016), epilepsy (Bernhardt et al., 2019), and agoraphobia (Indovina et al., 2019). Graph theory analyses have reported that patients suffering from CSVD exhibit increased path length and modularity and reduced small-worldness correlated with cognition in the global topology of functional brain networks (Schulz, Malherbe, Cheng, Thomalla, & Schlemm, 2021). For instance, a previous study (Wang et al., 2019) showed the role of disturbed small-world networks in patients with WM lesions and CI. Liu et al. (2019) revealed an altered reconfiguration pattern within/between the DMN and the executive control network (ECN) of CSVD patients. However, all of these studies investigate CSVD using either global network parameters or analysis of node topological properties. We combined the two aspects to provide more detailed information about functional changes across the whole brain. Furthermore, previous studies have mainly divided subjects into CSVD with and without CI or graded the severity of CI (Chen et al., 2019). To our knowledge, no graph theory study has separated CSVD patients with CMBs from those without CMBs.

Considering the research gaps and the severity of CMBs for CI, we aimed to investigate the topological organization of whole-brain

FC networks in CSVD patients with and without CMBs and their relation to clinical features. Briefly, we first used rs-fMRI to construct individual whole-brain, ROI-level FC networks and then investigated whether CSVD patients would show abnormal global and regional topological properties and whether nodal topological changes would significantly correlate with the clinical characteristics of CSVD patients.

2 | MATERIALS AND METHODS

2.1 | Subjects

Twenty-four CSVD-c patients (mean age: 67.54 ± 6.00 years, 10 females) and 42 CSVD-n patients (mean age: 66.33 ± 5.25 years, 22 females) were recruited from outpatient clinics at Shandong Provincial Hospital affiliated with Shandong First Medical University from September 2018 to June 2019. We also included 36 age- ($p = 0.646$, ANCOVA test) and sex- ($p = 0.646$, chi-square test) matched healthy subjects (mean age: 64.14 ± 8.57 years, 19 females) in our study.

According to a prior study (Liu, Wu, et al., 2019), the inclusion criteria for CSVD subjects were as follows: (a) age <75 years and (b) presence of signs of CSVD on MRI images, such as recent small subcortical infarcts, white matter hyperintensities (WMHs), lacunes, prominent perivascular spaces, CMBs, or/and atrophy on MRI. According to the Standards for Reporting Vascular Changes on Neuroimaging (STRIVE) criteria (Wardlaw, Smith, Biessels, et al., 2013), CMBs are defined as small round or ovoid areas of hypointense lesions that range in diameter from 2 to 5 mm and can be observed on T2*-weighted GRE or susceptibility-weighted sequences. In this research, CMBs were scored based on absence or presence, not number or location (Debette, Schilling, Duperron, Larsson, & Markus, 2019). Seven CSVD-c patients belong to lobar CMBs group and 17 CSVD-c patients are placed in deep CMBs group (Liu et al., 2020). WMHs were graded using Fazekas scale (0–3) and the number of lacunes was graded from 0 to 3 (0 = none, 1 = 1–2, 2 = 3–5, 3 =>5) (Fazekas, Chawluk, Alavi, Hurtig, & Zimmerman, 1987; Amin Al Olama et al., 2020).

The exclusion criteria were as follows: (a) coronary atherosclerosis, heart disease, (b) stroke due to atrial fibrillation, ventricular aneurysm, rheumatic immune system disease, vasculitis, drug abuse, or other suspicious causes, (c) symptomatic carotid artery stenosis (>50%) or asymptomatic carotid artery stenosis (>70%), (d) other neurological disorders, such as Alzheimer disease, Parkinson disease, and epilepsy, (e) prominent serious medical disease or cancer, (f) chronic kidney disease in stages 4–5 or bilateral renal artery stenosis, and (g) MRI contraindications.

2.2 | Cognitive assessment

All participants underwent the Montreal Cognitive Assessment (MoCA) Beijing version (www.mocatest.org), which is a one-page 30-point test administered in 10 min (Bergeron et al., 2017). The optimal cutoff for detecting cognitive impairment points was 13/14 for illiterate individuals, 19/20 for individuals with 1–6 years of education, and 24/25 for individuals with 7 or more years of education (Lu et al., 2011). In addition, a variety of executive functions, including flexibility, working memory, and inhibition, were also assessed using the Rey auditory verbal learning test (AVLT), which assesses verbal memory ability (Putcha et al., 2019); the symbol digit modalities test (SDMT), which evaluates attention and information processing speed (Benedict et al., 2017); the trail-making test (TMT), which evaluates attention, information processing speed, visual search and motor coordination (Wei et al., 2018); and the Stroop color-word test (SCWT) (Scarpina & Tagini, 2017). The examiner was professionally trained and qualified and had no knowledge of the subject grouping.

2.3 | Image acquisition

MRI scanning was performed on a MAGNETOM 3-Tesla MR scanner (Skyra, Siemens Healthcare, Erlangen, Germany). Before the scan, all participants maintained respiration and heart rate in a normal state. All participants were required to be awake and quietly breathing until the end of the scan. The resting-state functional scans were obtained with a gradient-echo echoplanar imaging sequence: TR/TE = 1500/30 ms, slice thickness = 3 mm, field of view (FOV) = 24 × 24 cm^2. SWI data were acquired using an three-dimensional T2*-weighted gradient echo sequence (TR/TE = 27/20 ms, slice thickness = 1.5 mm, and FOV = 22 × 22 cm^2). A three-dimensional T1-weighted (T1W) magnetization-prepared rapid acquisition gradient-echo sequence (TR/TE = 2300/2.32 ms, slice thickness = 0.9 mm, FOV = 24 × 24 cm^2) was performed for anatomic reference. In addition, T2-weighted (T2W) turbo spin echo, T2W fluid-attenuated inversion recovery (FLAIR), and diffusion-weighted images were acquired to detect brain abnormalities. Before the scan, all participants maintained respiration and heart rate in a normal state. All participants were required to be awake and quietly breathing until the end of the scan.

2.4 | Data preprocessing

Resting-state fMRI data reprocessing was performed using statistical parametric mapping (SPM8, http://www.fil.ion.ucl.ac.uk/spm) and Data Processing & Analysis for Resting-state Brain Imaging (DPABI Version 2.1, http://www.restfmri.net). The first 10 image volumes of functional images were removed for signal equilibrium and participant adaptation to the scanning noise. Then, the functional images were corrected for time offsets between slices and geometrical displacements due to head motion. We further calculated the mean frame-wise displacement (FD) to measure voxel-wise differences in motion in its derivation (Jenkinson, Bannister, Brady, & Smith, 2002). None of the participants were excluded based on the exclusion criteria of maximum head motion of 3.0 mm and 3.0°, with a mean FD > 0.2 mm. The T1-weighted images were coregistered to the average functional

images and then segmented into white matter (WM), gray matter (GM), and cerebrospinal fluid (CSF) by using the *New Segment* tool in DPABI. We removed linear trends and regressed out several nuisance signals from the time course of each voxel, including 24-parameter head-motion profiles (Friston, Williams, Howard, Frackowiak, & Turner, 1996; Yan et al., 2013), and the mean WM and CSF time series within the respective brain masks were derived from prior probability maps in SPM8 (threshold = 0.8). Subsequently, all the corrected functional data were normalized by the *DARTEL* (Ashburner, 2007) tool to Montreal Neurological Institute (MNI) space using an optimum 12-parameter affine transformation and nonlinear deformations and then resampled to a 3-mm isotropic resolution.

2.5 | Functional connectivity network construction

A region-based functional connectivity network was constructed as described in our previous study (Wen et al., 2018). Briefly, the automated anatomical labeling (AAL) template (Tzourio-Mazoyer et al., 2002) was used to segment registered fMRI time series into 90 cerebral cortex regions (Table 1). For each region, fMRI time series of all voxels lying in that region were averaged to obtain representative fMRI time series or BOLD signals of that region. Then, for each of the 90 ROIs, a mean time series was extracted, and Pearson correlation with all the other ROIs was calculated, therefore outputting a 90×90 correlation matrix. To exclude possible effects of spurious correlations between network nodes, a sparsity threshold (i.e., the ratio of the number of existing edges divided by the maximum possible number of edges in a network) was applied to individual correlation matrices to retain high correlations only. The sparsification approach normalized all resultant networks to have the same number of nodes and edges while minimizing the effects of discrepancies in the overall correlation strength between groups. To exclude the bias of a single sparse threshold, the correlation matrix for each subject was thresholded using the same sparsity ranging from 8% to 60% with an interval of 2% as our previous study (Wen et al., 2018), and the network metrics were calculated and then compared between groups at each sparsity.

2.6 | Network topological analysis

For the resultant networks at each sparsity threshold, both global and regional network topological properties were calculated using a graph theoretical network analysis toolbox (GRETNA v2.0, http://www.nitrc.org/projects/gretna; Wang et al., 2015). The global measures

TABLE 1 The 90 cortical and subcortical regions of interest defined in our study

Regions	Abbr.	Regions	Abbr.
Precentral gyrus	PreCG	Lingual gyrus	LING
Superior frontal gyrus, dorsolateral	SFGdor	Superior occipital gyrus	SOG
Superior frontal gyrus, orbital part	ORBsup	Middle occipital gyrus	MOG
Middle frontal gyrus	MFG	Inferior occipital gyrus	IOG
Middle frontal gyrus orbital part	ORBmid	Fusiform gyrus	FFG
Inferior frontal gyrus, opercular part	IFGoperc	Postcentral gyrus	PoCG
Inferior frontal gyrus, triangular part	IFGtriang	Superior parietal gyrus	SPG
Inferior frontal gyrus, orbital part	ORBinf	Inferior parietal, but supramarginal and angular gyri	IPL
Rolandic operculum	ROL	Supramarginal gyrus	SMG
Supplementary motor area	SMA	Angular gyrus	ANG
Olfactory cortex	OLF	Precuneus	PCUN
Superior frontal gyrus, medial	SFGmed	Paracentral lobule	PCL
Superior frontal gyrus, medial orbital	ORBsupmed	Caudate nucleus	CAU
Gyrus rectus	REC	Lenticular nucleus, putamen	PUT
Insula	INS	Lenticular nucleus, pallidum	PAL
Anterior cingulate and paracingulate gyri	ACG	Thalamus	THA
Median cingulate and paracingulate gyri	DCG	Heschl gyrus	HES
Posterior cingulate gyrus	PCG	Superior temporal gyrus	STG
Hippocampus	HIP	Temporal pole: superior temporal gyrus	TPOsup
Parahippocampal gyrus	PHG	Middle temporal gyrus	MTG
Amygdala	AMYG	Temporal pole: middle temporal gyrus	TPOmid
Calcarine fissure and surrounding cortex	CAL	Inferior temporal gyrus	ITG
Cuneus	CUN		

included five small-world property metrics and two network efficiency metrics. The regional measure used in this study was nodal betweenness centrality (BC). Table 2 shows the general descriptions of the network properties.

$$B_{\text{nodal}}(i) = \sum_{s \neq i \neq t \in G} \frac{e_{st}(i)}{e_{st}} \quad (1)$$

where $e_{st}(i)$ denotes the number of shortest paths in network G between node s and node t, which pass through node i, while e_{st} denotes the total number of shortest paths in network G between node s and node t. $B_{\text{nodal}}(i)$ measures the fraction of all shortest paths that pass through a given node i. Node i was considered a brain hub if $B_{\text{nodal}}(i)$ was at least 1 SD greater than the mean nodal BC of the whole network (i.e., $B_{\text{nodal}}(i)$ > mean + SD).

As the global and local topological properties were calculated for each sparsity threshold, we calculated the area under the curve (AUC) for each topological property (for the illustration of AUC, see Figure S1, Supporting Information) over the range of sparsity (0.08–0.6) to provide a summarized scalar independent of single threshold selection (Wen et al., 2018; Zhang, Liu, Chen, Liu, & Wang, 2015). The graph theory analysis in our study was implemented using a graph theoretical network analysis toolbox (GRETNA, http://www.nitrc.org/projects/gretna/; Wang et al., 2015).

TABLE 2 Global and local topological properties used in the study

Global network properties	
Global efficiency, E_{glob}	E_{glob} is defined as the mean value of all regions' global efficiency.
Local efficiency, E_{loc}	E_{loc} is defined as the mean value of all regions' local efficiency.
Shortest path length, L_p	L_p is defined as the average length of the shortest path between every two nodes in network G, which quantifies the ability for information to be propagated in parallel.
Clustering coefficient, C_p	C_p is the average clustering coefficient over all nodes, which indicates the extent of local interconnectivity or cliquishness in a network
Normalized L_p (λ)	$\lambda = {L_p}^{\text{real}}/{L_p}^{\text{rand}}$, ${L_p}^{\text{rand}}$ is the mean shortest path length of 100 matched random networks.
Normalized C_p (γ)	$\gamma = {C_p}^{\text{real}}/{C_p}^{\text{rand}}$, ${C_p}^{\text{rand}}$ is the mean clustering coefficient of 100 matched random networks.
Small-worldness, σ	$\sigma = \lambda/\gamma$, A real network would be considered small world if $\gamma > 1$ and $\lambda \approx 1$.
Local nodal properties	
Nodal betweenness	$B_{\text{nodal}}(i)$ is defined as the fraction of all shortest paths in the network
Centrality $B_{\text{nodal}}(i)$	G that pass through a given node i, the mathematical definition is presented in Equation (1)

2.7 | Between-group statistical comparison and correlation analysis

To assess whether there were significant differences in the topological properties of the functional brain networks across the CSVD-c, CSVD-n, and control groups, one-way analysis of variance (ANOVA) was performed to compare the AUC value of each network metric (global and nodal properties) among the three groups, and a pairwise post hoc test via the least-significant difference (LSD) method was subsequently used to identify significant intergroup differences. The chi-square test was used to analyze the sex ratios among the three groups, with ANOVA used for other clinical parameters. Once significant intergroup differences were identified in any regional topological metrics, we further assessed the correlations between these metrics and clinical parameters in the CSVD-c and CSVD-n groups. A partial correlation analysis was used to test the association with age, sex, and mean FD as the covariates. Because these analyses were exploratory in nature, we used a statistical significance level of $p < 0.05$.

3 | RESULTS

3.1 | Demographic and clinical characteristics of the subjects

The demographic and clinical characteristics of each group are summarized in Table 3. The CSVD-c group had significantly lower MoCA, AVLT, and SDMT scores and significantly higher SCWT and TMT scores than the other groups. No significant differences were found in age, sex, years of education, body mass index (BMI), or mean FD between the patient and control groups.

3.2 | Alterations in the global properties of functional networks in CSVD

Over the sparsity range of 0.08–0.60 (step = 0.02), the CSVD-c, CSVD-n, and control groups all exhibited high-efficiency small-world topology characterized by $\gamma > 1$, $\lambda \approx 1$, and $\sigma = \gamma/\lambda > 1$ (Figure 1). Statistical comparisons (ANOVA with LSD post hoc test) were performed to detect significant differences in global properties among the three groups. Compared to the CSVD-n and control groups, the CSVD-c group showed a significantly ($p < 0.05$) decreased global efficiency (E_{glob}), local efficiency (E_{loc}), and clustering coefficient (C_p) and increased shortest path length (L_p) over a wide range of sparsity thresholds (Figure 1). No significant difference was found between the CSVD-n group and the control group. Moreover, the CSVD-c group showed significantly ($p < 0.05$) decreased AUC values of E_{glob}, E_{loc}, and C_p and increased L_p (Table 4), indicating the consistency and robustness of significant alterations over sparsity thresholds. There was no significant difference in other global properties among groups.

TABLE 3 Demographic and clinical characteristics of CSVD patients and controls

Characteristics	CSVD-c	CSVD-n	Controls	*p*-Value	*p*-Value (post hoc)		
					G1 versus G3	G1 versus G2	G2 versus G3
Gender	14M/10F	20M/22F	17M/19F	0.646$^{\chi 2}$	-	-	-
Age (years)	67.54 ± 6.00	66.33 ± 5.25	64.14 ± 8.57	0.140[a]	-	-	-
Education (years)	11.33 ± 2.87	11.43 ± 2.41	12.72 ± 3.44	0.093[a]	-	-	-
BMI	26.26 ± 3.37	24.68 ± 3.26	25.42 ± 2.85	0.147[a]	-	-	-
Smoking, *n* (%)	7 (29)	8 (19)	10 (28)	-	-	-	-
Hypertension, *n* (%)	22 (92)	36 (86)	12 (33)	<0.001$^{\chi 2}$	-	-	-
Diabetes, *n* (%)	9 (38)	8 (19)	4 (11)	0.044$^{\chi 2}$	-	-	-
Hyperlipidemia, *n* (%)	15 (63)	13 (31)	5 (14)	<0.001$^{\chi 2}$	-	-	-
MoCA	25.52 ± 2.82	27.55 ± 0.89	28.66 ± 0.87	**<0.001**[a]	**<0.001**	**<0.001**	**0.002**
AVLT	54.48 ± 16.91	64.93 ± 9.55	68.14 ± 8.47	**<0.001**[a]	**<0.001**	**0.001**	N.S.
SDMT	23.26 ± 10.94	30.22 ± 9.05	39.63 ± 14.32	**<0.001**[a]	**<0.001**	**0.023**	**0.001**
SCWT	187.13 ± 71.17	145.90 ± 27.55	134.83 ± 38.12	**<0.001**[a]	**<0.001**	**0.001**	N.S.
TMT-A + B	346.17 ± 175.25	259.78 ± 76.34	213.26 ± 101.20	**<0.001**[a]	**<0.001**	**0.005**	N.S.
FD_Jenkinson	0.13 ± 0.07	0.13 ± 0.08	0.11 ± 0.44	0.339[a]	-	-	-
WMHs	1.96 ± 0.91	1.57 ± 0.70	-	0.057 [b]	-	-	-
Lacunes	0.88 ± 0.99	0.05 ± 0.22	-	<0.001[b]	-	-	-

Abbreviations: AVLT, sum of Rey Auditory Verbal Learning Test (N1-7); BMI, body mass index; CSVD, cerebral small vessel disease; CSVD-c, CSVD with CMBs; CSVD-n, CSVD without CMBs; FD_Jenkinson, frame-wise displacement (Jenkinson et al., 2002); G1, CSVD-c group; G2, CSVD-n group; G3, control group; MoCA, Montreal Cognitive Assessment; N.S., not significant; SCWT, sum of Stroop Color-Word Test (stroop1-3); SDMT, Symbol Digit Modalities Test; TMT, the Trail-Making Test; TMT A + B, sum of TMT-A and TMT-B; χ^2, chi-square test; WMHs, white matter hyperintensities.
[a]ANOVA test.
[b]Wilcoxon test.

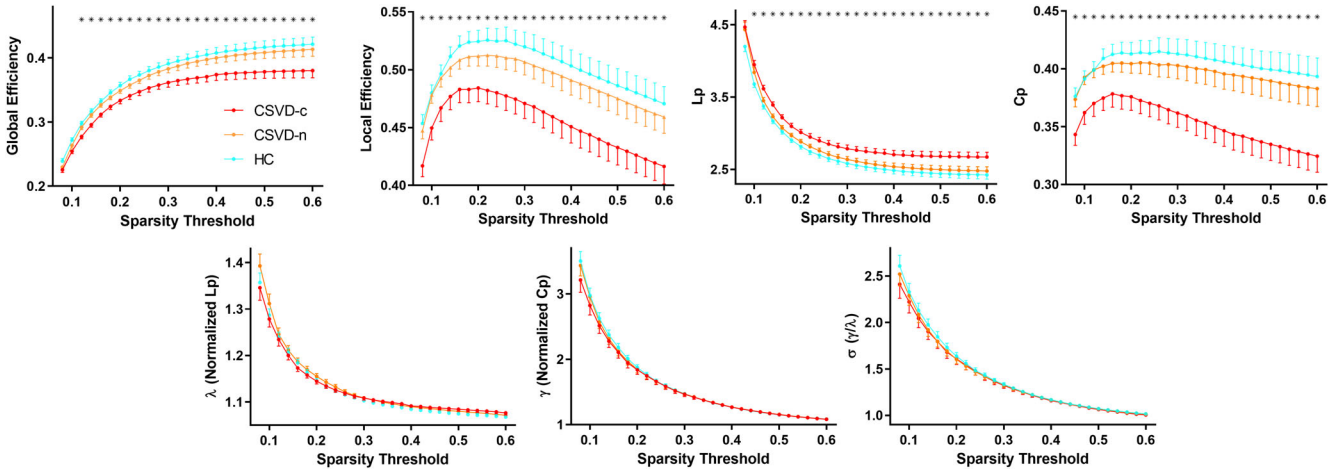

FIGURE 1 Differences in global topological properties of functional networks among the three groups. Data points marked with a star indicate significant ($p < 0.05$, ANOVA with LSD post hoc test) intergroup differences in the global network metric under a corresponding sparsity threshold

3.3 | Hub distributions of functional networks in CSVD

For each group, the nodes were considered brain hubs if their nodal BC was at least 1 SD greater than the average value (Wen et al., 2018). We found highly similar hub distributions among groups, with common regions mainly in the bilateral temporal pole (TPOsup), middle temporal gyrus (MTG), inferior temporal gyrus (ITG), right supplementary motor area (SMA), median cingulate and paracingulate gyri (DCG), superior temporal gyrus (STG), and left middle occipital gyrus (MOG). Compared with the control group, the CSVD-c group had two additional hub regions in the left middle frontal gyrus (MFG) and

fusiform gyrus (FFG) and lacked the left DCG as the hub region, while the CSVD-n group had two additional hub regions in the right inferior frontal gyrus, orbital part (ORBinf), and left STG and lacked the right FFG as a hub region (Table 5, Figure 2).

3.4 | Alterations in the regional properties of functional networks in CSVD

Nine brain regions exhibiting significantly (ANOVA tests, $p < 0.05$) altered nodal BC among the three groups were identified and were mainly located in the DMN, attention, and visual-related functional modules (Table 6). Furthermore, using the LSD post hoc test, pairwise intergroup differences were also identified. Compared with the control group, the CSVD-c group exhibited significantly decreased nodal BC in the right ORBsup and PCG and increased nodal BC in the right anterior cingulate and paracingulate gyri (ACG) and the left MFG, cuneus, and angular gyrus, while the CSVD-n group exhibited significantly increased nodal BC in the left insula. In addition, the CSVD-c group exhibited significantly decreased nodal BC in the left IFGoperc and increased nodal BC in the left MFG, hippocampus and angular gyrus compared with the CSVD-n group (Figure 3). Notably, the regions that exhibited significantly reduced nodal BC in both the CSVD-c and CSVD-n groups were not hub regions.

3.5 | Correlations between network topological alterations and clinical parameters

By performing partial correlation analysis, we found that the nodal BC of the right PCG showed a significantly positive correlation ($r = 0.456$, $p = 0.038$) with the SDMT and that the left cuneus showed a significantly positive correlation ($r = 0.510$, $p = 0.018$) with AVLT scores (Figure 4a) in the CSVD-c group. In addition, the nodal BC of the right

TABLE 4 Group comparisons of AUC values of global network properties

Group	E_{glob}	E_{loc}	L_p	C_p	λ	γ	σ
CSVD-c	0.348 ± 0.035	0.453 ± 0.061	2.947 ± 0.240	0.352 ± 0.056	1.589 ± 0.216	1.128 ± 0.025	1.389 ± 0.179
CSVD-n	0.371 ± 0.042	0.490 ± 0.069	2.790 ± 0.275	0.396 ± 0.071	1.609 ± 0.230	1.132 ± 0.034	1.401 ± 0.198
HC	0.379 ± 0.042	0.501 ± 0.070	2.722 ± 0.254	0.404 ± 0.071	1.621 ± 0.209	1.125 ± 0.027	1.418 ± 0.150
p-Value (ANOVA)	**0.021***	**0.033***	**0.007***	**0.018***	0.849	0.539	0.823
p-Value (CSVD-c vs. HC)	**0.006***	**0.011***	**0.002***	**0.006***	-	-	-
p-Value (CSVD-n vs. HC)	0.404	0.468	0.260	0.580	-	-	-
p-Value (CSVD-c vs. CSVD-n)	**0.034***	**0.043***	**0.022***	**0.018***	-	-	-

Abbreviations: ANOVA, analysis of variance; AUC, area under the curve; CSVD, cerebral small vessel disease; HC, healthy controls.
*$p < 0.05$ (ANOVA, LSD post-hoc test).

TABLE 5 Hub regions of functional networks in both CSVD and control groups

CSVD-c		CSVD-n		HC	
Regions	B_{nodal}	Regions	B_{nodal}	Regions	B_{nodal}
SMA.R	74.78 ± 61.24	SMA.R	59.04 ± 40.90	SMA.R	62.64 ± 70.21
DCG.R	64.96 ± 51.08	DCG.R	65.90 ± 47.95	DCG.R	72.70 ± 62.56
MOG.L	72.75 ± 80.34	MOG.L	83.60 ± 66.89	MOG.L	81.34 ± 65.13
STG.R	68.21 ± 56.49	STG.R	72.43 ± 54.56	STG.R	81.02 ± 60.96
TPOsup.L	62.80 ± 59.51	TPOsup.L	67.20 ± 50.79	TPOsup.L	82.77 ± 77.46
TPOsup.R	67.93 ± 63.83	TPOsup.R	62.12 ± 45.47	TPOsup.R	81.50 ± 57.73
MTG.L	100.11 ± 82.55	MTG.L	91.42 ± 68.35	MTG.L	93.85 ± 74.93
MTG.R	71.56 ± 47.22	MTG.R	65.77 ± 50.39	MTG.R	66.54 ± 69.76
ITG.L	76.59 ± 59.14	ITG.L	64.36 ± 57.06	ITG.L	66.48 ± 52.90
ITG.R	83.29 ± 65.71	ITG.R	90.26 ± 72.43	ITG.R	115.86 ± 89.99
FFG.L	74.15 ± 70.93	**STG.L**	58.47 ± 39.18	**FFG.R**	64.01 ± 57.42
FFG.R	57.33 ± 62.16	**ORBinf.R**	59.08 ± 59.67	**DCG.L**	70.68 ± 55.31
MFG.L	64.54 ± 40.49	**DCG.L**	71.61 ± 55.36		

Abbreviations: B_{nodal} represents the AUC value (mean ± SD) of nodal betweenness centrality across thresholds; CSVD, cerebral small vessel disease; HC, healthy control.

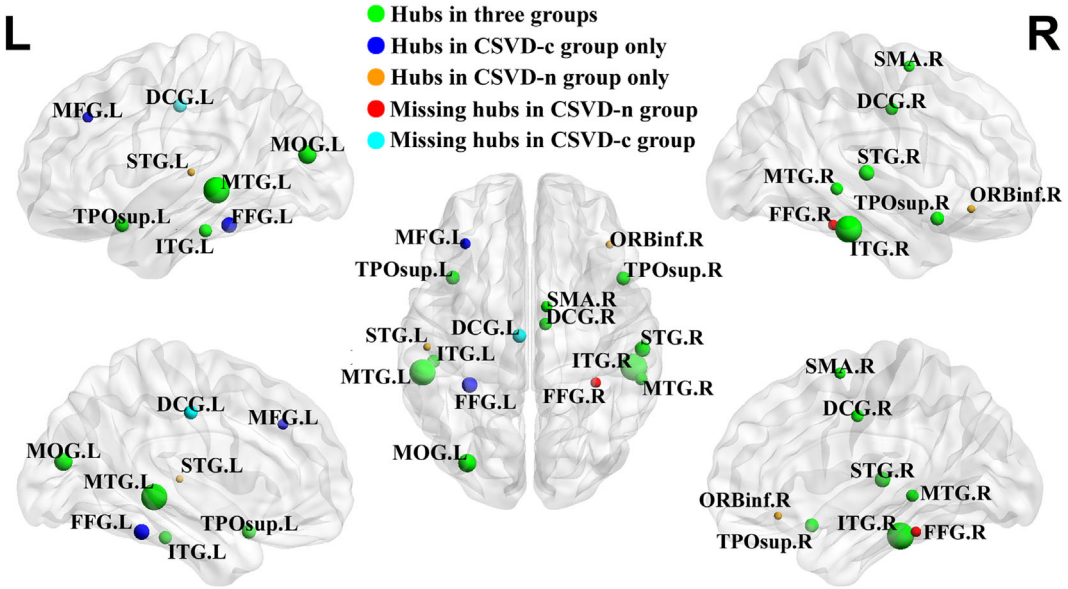

FIGURE 2 Hub region distributions of the functional networks for both groups. The hub nodes are shown with different node sizes, indicating their nodal betweenness centrality values. The brain graphs were visualized by using *BrainNet Viewer* software (http://www.nitrc.org/projects/bnv/). For the abbreviations of the nodes, see Table 1

TABLE 6 Brain regions showing significantly altered nodal betweenness centrality among three groups for functional networks

Module	Region	B_{nodal}			*p*-Value (ANOVA)	*p*-Value (post-hoc)		
		CSVD-c	CSVD-n	Control		G1 versus G3	G1 versus G2	G2 versus G3
DMN	ORBsup.R	23.56 ± 19.79	39.22 ± 33.64	53.85 ± 47.50	**0.009**	**0.002**	N.S.	N.S.
Attention	MFG.L	64.54 ± 41.36	43.73 ± 38.93	39.28 ± 32.28	**0.032**	**0.012**	**0.032**	N.S.
Attention	IFGoperc.L	19.09 ± 14.80	38.75 ± 40.98	25.34 ± 27.77	**0.039**	N.S.	**0.018**	N.S.
Sensory/motor	INS.L	39.08 ± 34.88	44.55 ± 46.92	25.21 ± 28.69	**0.046**	N.S.	N.S.	**0.016**
DMN	ACG.R	41.71 ± 48.32	27.47 ± 30.29	22.46 ± 27.54	**0.044**	**0.015**	N.S.	N.S.
DMN	PCG.R	15.10 ± 18.90	21.45 ± 21.29	29.82 ± 35.26	**0.045**	**0.016**	N.S.	N.S.
Subcortical	HIP.L	37.79 ± 30.32	16.59 ± 25.85	27.86 ± 42.68	**0.047**	N.S.	**0.016**	N.S.
Vision	CUN.L	40.15 ± 34.63	29.01 ± 42.20	18.03 ± 20.94	**0.041**	**0.014**	N.S.	N.S.
Attention	ANG.L	41.10 ± 42.78	26.39 ± 21.35	22.17 ± 20.54	**0.032**	**0.011**	**0.040**	N.S.

Note: The modular division of brain regions is based on previous study (Yong et al., 2009).
Abbreviations: ANOVA, analysis of variance; B_{nodal} represents the AUC values (mean ± SD) of the nodal betweenness centrality of each group; CSVD, cerebral small vessel disease; DMN, default mode network; G1, CSVD with CMBs (CSVD-c) group; G2, CSVD without CMBs (CSVD-n) group; G3, control group, N.S., not significant.

ACG showed a significantly positive correlation ($r = 0.381$, $p = 0.017$) with the SDMT, and the right PCG showed a significantly negative correlation ($r = -0.344$, $p = 0.032$) with TMT scores (Figure 4b) in the CSVD-n group.

4 | DISCUSSIONS

The present study is, to our knowledge, the first to apply graph theory approaches to compare differences in the topological organization of functional brain networks in CSVD patients with and without CMBs. Our findings revealed the following: (a) at the global level, although both the CSVD and control groups showed small-world properties of the FC networks, the CSVD-c group showed a significantly decreased clustering coefficient and global/local efficiency and an increased shortest path length. (b) At the regional level, although both groups showed highly similar hub distributions, CSVD-c patients exhibited significantly altered nodal BC in the DMN and attention, and visual-related functional areas compared to CSVD-n patients and controls. There was almost no nodal alteration between CSVD-n patients and controls. (c) Altered nodal BC of the right anterior/posterior cingulate gyrus and left cuneus were significantly correlated with the clinical cognitive parameters of CSVD patients, indicating potential bio-markers of CSVD.

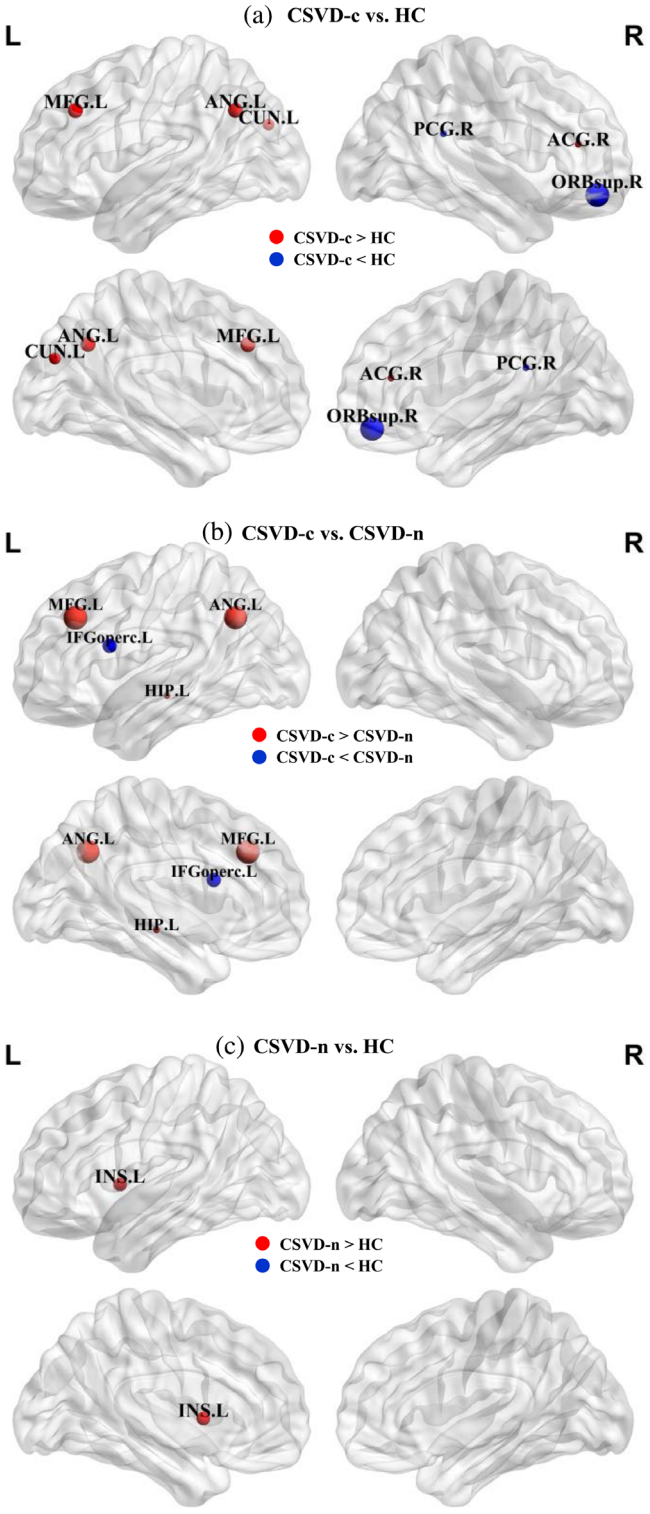

FIGURE 3 The differences in nodal betweenness centrality of the functional networks across the CSVD-c, CSVD-n, and HC groups. The disrupted nodes with significantly decreased or increased nodal betweenness centrality are shown in blue or red, and the scaled node sizes indicate the *F* values of ANOVA. For the abbreviations of the nodes, see Table 1

An early study (Telesford, Joyce, Hayasaka, Burdette, & Laurienti, 2011) proved that the human brain is represented by a small-world network, which is characterized by high local clustering and a low shortest path length. Here, we found that the functional brain networks of both CSVD patients and controls exhibited a small-world architecture, showing that the brain functional networks were reliably constructed. Previous studies (Wang et al., 2019; Yi et al., 2015) showed the preservation of a small-world architecture in a healthy population and in the presence of pathology, which could provide a certain important reference for our study. Compared with CSVD-n patients and controls, CSVD-c patients showed less specialized or segregated network organization characterized by significantly decreased network efficiency and lower clustering. Decreased E_{glob} means decreased information transfer between remote regions, which is predominantly related to long-range connections. And E_{loc} is mainly associated with the short-range connections between neighboring regions. These changes indicate disrupted topological organization of the FC networks in CSVD-c patients, which can be attributed to affected FC. Several rs-fMRI studies (Sun et al., 2011; Zhou et al., 2016) showed decreased FC between posterior components of the DMN and the medial PFC in patients with CSVD. Clustering measures the tendency of regions to join other regions to form a clique of densely interconnected neighbors, reflecting the extent of local cliquishness. From the perspective of information dissemination, higher clustering suggests higher efficiency for local information transfer, and a shorter characteristic path length means high efficiency in global information transmission (Liao, Vasilakos, & He, 2017). These reflect an optimal balance between local specialization and global integration, which is the outcome of natural selection (Liao et al., 2017). The lower clustering and increased shortest path length in CSVD patients could represent less optimal organization of the brain functional networks. Notably, however, this significant difference did not persist between the CSVD-n and control groups. From the aspect of histopathologic correlates, existing studies and animal experiments (Schreiber, Bueche, Garz, & Braun, 2013; Wardlaw, Smith, & Dichgans, 2013; Zhang et al., 2017) have described diffuse cerebrovascular endothelial failure as the starting point of CSVD-related brain injury. Endothelial failure drives blood–brain barrier (BBB) dysfunction, resulting in increased permeability and leakage of potentially harmful toxins and immune cells into surrounding brain tissues, which leads to inflammation in the brain. Moreover, CMBs are more likely to be induced by systemic inflammation, implying more severe pathological processes (Ahn, Anrather, Nishimura, & Schaffer, 2018). Higher levels of inflammatory markers were found in patients with CMBs (Miwa et al., 2011), and notably, E-selectin and VEGF, two important markers of endothelial damage, are shown to be related only to CMBs but not other markers of CSVD (Low, Mak, Rowe, Markus, & O'Brien, 2019). This is capable of leading to more severe disruptions of the neurovascular unit, including neuronal dysfunction and cell death (Iadecola, 2017).

As the targeted codes in neurodegenerative diseases, hub regions interact with many brain regions, thereby playing a key role in the brain networks (van den Heuvel & Sporns, 2013). If the core nodes are attacked, the efficiency and stability of network information processing and transmission will be significantly reduced. Given that BC reflects the central roles of nodes in the overall information

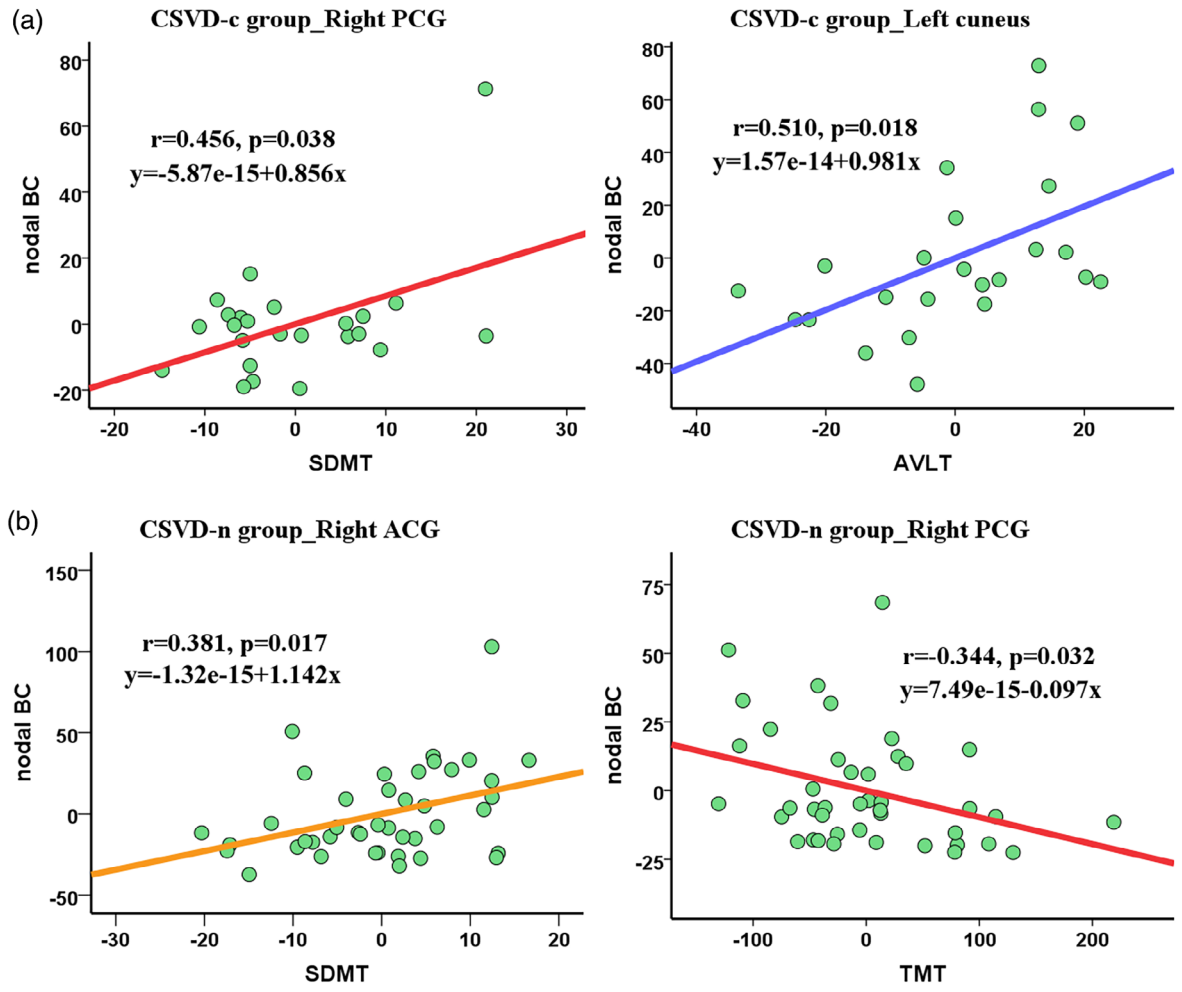

FIGURE 4 Correlations between nodal topological properties and clinical parameters. Of note, the coordinate values of both the *X* axis (clinical parameter) and *Y* axis (nodal BC) do not reflect the initial values of these variables when considering age, sex and mean FD as covariates. For the abbreviations of the nodes, see Tables 1 and 3

communication of the networks and has been extensively utilized in the hub analysis of brain networks (Wang, Li, Wang, Xian, & He, 2016; Zhang et al., 2020), we defined the hub regions of brain FC networks by identifying the nodal BC as the key index. We found similar global hub distributions among groups, suggesting that these key regions in brain networks are conserved throughout the development process and that small-world networks can tolerate developmental alterations or disease (Wen et al., 2017). Moreover, partial reorganization was observed in CSVD patients and can be interpreted as a balancing effect. Compared with the controls, the CSVD-c group lacked the left DCG as the hub region, the CSVD-n group lost the right FFG as a hub node, and four new core nodes appeared. DCG has been associated with cognitive control processes (Shackman et al., 2011). A previous study (Yi et al., 2015) reported a decreased within-module degree in the DCG in patients with subcortical vascular mild cognitive impairment (MCI), and another study (Schaefer et al., 2014) recruiting early CSVD patients used eigenvector centrality (EC) to reveal decreased connectivity in the bilateral DCG, which provides support for our findings. The function of the FFG is now considered a key role for functionally specialized computations of high-level vision, including face perception, reading, and object recognition (Weiner & Zilles, 2016). In an rs-fMRI study (Cai et al., 2015), altered FC of the FFG was reported in patients with amnestic MCI. And the literature on right-brain stroke (Chen, Hartman, Priscilla Galarza, & DeLuca, 2012) implied that the central role of the right IFG involves promoting the global processing of visuospatial perception. Moreover, in a combined analysis of functional networks and structural connectivity, the authors demonstrated that functional recruitment in the FFG and IFG are specifically targeted for visuoperceptual working memory tasks, and in the visuospatial working memory task, the axial diffusivity and fractional anisotropy of the white matter bundles connecting the FFG and IFG are related to processing speed (Sala-Llonch, Palacios, Junqué, Bargalló, & Vendrell, 2015). Of note, in the present study, we found that the absent right FFG and additional right IFG were hub regions in CSVD-n patients compared with controls. We thus assumed that CSVD might change the function of the right FFG, which might be compensated by the right IFG.

We also revealed the distributed regions with altered nodal BC in the CSVD groups, and the involved regions were categorized into DMN, sensorimotor, attention, and visual association functions.

The disrupted regions in the DMN mainly involved the right PCG, ORBsup, and ACG. The DMN is considered the vital module involved in higher cognition, especially in internally directed, self-relevant cognition (Buckner, Andrews-Hanna, & Schacter, 2008; Raichle, 2015), attention level, and theory of mind (Mevel et al., 2010). Specific changes in the DMN have been reported in CSVD patients in the literature (Chen et al., 2019; Liu, Wu, et al., 2019; Staffaroni et al., 2018; Yi et al., 2012). As the core hub for the posterior subnetwork of the DMN, the PCG plays a crucial role in the retrieval of episodic memory, integration of self-relative information, and autobiographical search (Qiu et al., 2021). In a cohort of early CSVD subjects without dementia, patients suffering from a more severe disease state exhibited reduced EC in the PCC (Schaefer et al., 2014). Interestingly, a combined analysis involving 1,351 patients and 1,097 healthy control subjects reported reduced metabolism and perfusion in the PCG in Alzheimer disease and prodromal MCI (Schroeter, Stein, Maslowski, & Neumann, 2009). In particular, Alzheimer disease is often related to CSVD. Thus, our findings, the correlations between the nodal BC of the right PCG and SDMT as well as TMT scores, may provide neuroimaging evidence of impairments of cognition and attention in patients with CSVD. The ACG is an important brain region associated with attentional control, memory processing, and emotional processing (Bush, Luu, & Posner, 2000; Miotto et al., 2020). Heflin et al. (2011) demonstrated that combined with Stroop performance and structural MRI, reduced ACG function predicted poor attentional control and a greater tendency to make mistakes. In the present study, we found that the nodal BC of the right ACG showed a significantly positive correlation with SDMT scores, which is consistent with previous findings. Similarly, in an rs-fMRI study (Ding et al., 2017), ReHo in the anterior DMN decreased and that in the posterior DMN increased in patients with ischemic WMLs. In this study, we deduce that the increased BC in the right ACG may represent a compensatory effect in CI. Owing to vascular damage, reallocation or recruitment of cognitive resources against CI are needed in CSVD patients to maintain normal levels of cognition.

Serving as the sensory-motor functional area, the insula is associated with multiple functions, such as motor control, perception, self-awareness, and cognitive function (Boccardi et al., 2005; Uddin, Nomi, Hébert-Seropian, Ghaziri, & Boucher, 2017). Sridharan, Levitin, and Menon (2008) revealed that the dorsal anterior insula exerted stronger causal influences on other brain networks, including the DMN, especially in relation to underlying social cognitive processes, and that this could be the interpretation of increased BC of the left insula in CSVD patients compared with control subjects.

Attention networks with increased nodal BC mainly involved the left MFG, angular gyrus, and IFGoperc, all of which are interestingly distributed in the left cerebral hemisphere. The angular gyrus serves as a key region in attention functional areas and is engaged in mediating automatic bottom-up attentional resources and monitoring episodic memory retrieval (Cabeza, Ciaramelli, Olson, & Moscovitch, 2008; Seghier, 2013). An early study (Ding et al., 2017) showed increased ReHo in the bilateral angular gyrus in patients with ischemic WMLs. We speculate that this may reflect a shift in the balance of attention networks.

The cuneus participates in visual–spatial processing and acts as the core region of the WM processing system assigned a visual–spatial sketchpad (Chai, Abd Hamid, & Abdullah, 2018; Qin, Xuan, Liu, Jiang, & Yu, 2015). A recent study reported a significant association between left cuneus gray volume and WM performance (He et al., 2021), which could provide a certain important reference for our finding on the correlation between nodal BC and AVLT scores.

In this study, compared with the CSVD-n group, the CSVD-c group exhibited significantly increased nodal BC in the left hippocampus. In other words, CMBs may damage the hippocampus to some extent. The hippocampus is an important brain region that is responsible for the body's cognitive functions, especially memory and learning ability (Lisman et al., 2017). Anouk et al. demonstrated the influence of CMBs at different locations on cognition. CMBs in the frontal and temporal lobes are associated with CI in nondemented elderly patients, independent of coexisting lesions related to other CSVDs (van Norden et al., 2011). Damage to vascular integrity and the BBB found in WMHs leads to neuronal damage to the hippocampus (Young, Halliday, & Kril, 2008), and the process by which CMBs occur also has similar pathological changes (Pantoni, 2010). Thus, we reasonably infer that CMBs may impair the hippocampus, leading to cognitive decline in CSVD-c patients. We did not observe correlates between nodal BC in the hippocampus and cognitive scores, and we suspect that the patients' lesions were mild or that there was a nonlinear correlation between the two. More neuroimaging studies should be conducted to test this hypothesis.

The present study has several limitations. First, our study had a cross-sectional design, and the sample size was relatively small. In large-scale epidemiologic studies, CMBs incidence ranges from 5% to 35% in aging participants (age >45 years) (Haller et al., 2018). The low prevalence of CMBs limits statistical power. More cases and follow up observations will be included in future studies. Second, the location and number of CMBs will be taken into account in future studies because of their effect on cognition. Furthermore, although the AAL template is still widely used in constructing human brain organizations, different parcellation strategies may result in considerable differences in the graph theory metrics (Wang et al., 2009). Different parcellation schemes will be included to test the reproducibility of our findings.

5 | CONCLUSION

In our study, we used whole-brain ROI-level FC analysis and graph theory analysis to investigate the altered topological organization of FC networks in CSVD. Compared to CSVD-n patients and controls, CSVD-c patients showed significantly altered global and nodal topological properties, while there was almost no topological alteration

between CSVD-n patients and controls. And the altered nodal BC mainly distributed in the DMN, sensorimotor, attention, and visual functional areas. Particularly, the altered nodal BC of the right anterior/posterior cingulate gyrus and left cuneus were significantly correlated with cognitive parameters in CSVD patients. These results suggest that CSVD patients with and without CMBs had segregated disruptions in the topological organization of the intrinsic functional brain network, which may be due to different etiological contributions. These findings may extend our understanding of how functional disruptions of neuronal circuits are linked to the pathophysiology of CSVD.

ACKNOWLEDGMENTS

The authors thank all of the volunteers and patients for their participation in our study. This work was supported by grants from the National Natural Science Foundation of China (32100902), the Fundamental Research Funds for the Central Universities (SWU118065), the Technology Development Plan of Jinan (201301049, 201602206, 201907052), Medical and Health Science and Technology Development Project of Shandong Province (2016WS0529, 2019WS544) and Funding for Study Abroad Program by Shandong Province (201803059), Shandong Provincial Natural Science Foundation (ZR2020MH288).

CONFLICT OF INTEREST

The authors declare that they have no competing interests.

AUTHOR CONTRIBUTIONS

Haotian Xin and Hongwei Wen wrote the main manuscript text. Hongwei Wen prepared Figures 1-4. Mengmeng Feng, Yian Gao, Chaofan Sui, and Nan Zhang prepared the clinical data and imaging data. Lingfei Guo and Changhu Liang revised the main manuscript text. All authors reviewed the manuscript.

DATA AVAILABILITY STATEMENT

The data that support the findings of this study are available from the corresponding author upon reasonable request.

ORCID

Haotian Xin https://orcid.org/0000-0001-8781-1815
Hongwei Wen https://orcid.org/0000-0003-1717-7235
Mengmeng Feng https://orcid.org/0000-0001-5349-2780
Yian Gao https://orcid.org/0000-0002-3444-3382
Chaofan Sui https://orcid.org/0000-0002-1049-3772
Nan Zhang https://orcid.org/0000-0002-6202-9349
Changhu Liang https://orcid.org/0000-0003-3796-2978
Lingfei Guo https://orcid.org/0000-0002-4885-625X

REFERENCES

Ahn, S. J., Anrather, J., Nishimura, N., & Schaffer, C. B. (2018). Diverse inflammatory response after cerebral microbleeds includes coordinated microglial migration and proliferation. *Stroke*, *49*, 1719–1726.

Al Olama, A. A., Wason, J. M. S., Tuladhar, A. M., van Leijsen, E. M. C., Koini, M., Hofer, E., … Markus, H. S. (2020). Simple MRI score aids prediction of dementia in cerebral small vessel disease. *Neurology*, *94*, e1294–e1302.

Ashburner, J. (2007). A fast diffeomorphic image registration algorithm. *NeuroImage*, *38*, 95–113.

Benedict, R. H., DeLuca, J., Phillips, G., LaRocca, N., Hudson, L. D., & Rudick, R. (2017). Validity of the symbol digit modalities test as a cognition performance outcome measure for multiple sclerosis. *Multiple Sclerosis*, *23*, 721–733.

Bergeron, D., Flynn, K., Verret, L., Poulin, S., Bouchard, R. W., Bocti, C., … Laforce, R., Jr. (2017). Multicenter validation of an MMSE-MoCA conversion table. *Journal of the American Geriatrics Society*, *65*, 1067–1072.

Bernhardt, B. C., Fadaie, F., Liu, M., Caldairou, B., Gu, S., Jefferies, E., … Bernasconi, N. (2019). Temporal lobe epilepsy: Hippocampal pathology modulates connectome topology and controllability. *Neurology*, *92*, e2209–e2220.

Boccardi, M., Sabattoli, F., Laakso, M. P., Testa, C., Rossi, R., Beltramello, A., … Frisoni, G. B. (2005). Frontotemporal dementia as a neural system disease. *Neurobiology of Aging*, *26*, 37–44.

Buckner, R. L., Andrews-Hanna, J. R., & Schacter, D. L. (2008). The brain's default network: Anatomy, function, and relevance to disease. *Annals of the New York Academy of Sciences*, *1124*, 1–38.

Bush, G., Luu, P., & Posner, M. I. (2000). Cognitive and emotional influences in anterior cingulate cortex. *Trends in Cognitive Sciences*, *4*, 215–222.

Cabeza, R., Ciaramelli, E., Olson, I. R., & Moscovitch, M. (2008). The parietal cortex and episodic memory: An attentional account. *Nature Reviews. Neuroscience*, *9*, 613–625.

Cai, S., Chong, T., Zhang, Y., Li, J., von Deneen, K. M., Ren, J., … Huang, L. (2015). Altered functional connectivity of fusiform gyrus in subjects with amnestic mild cognitive impairment: A resting-state fMRI study. *Frontiers in Human Neuroscience*, *9*, 471.

Chai, W. J., Abd Hamid, A. I., & Abdullah, J. M. (2018). Working memory from the psychological and neurosciences perspectives: A review. *Frontiers in Psychology*, *9*, 401.

Chen, H., Li, Y., Liu, Q., Shi, Q., Wang, J., Shen, H., … Zhang, Y. M. (2019). Abnormal interactions of the salience network, central executive network, and default-mode network in patients with different cognitive impairment loads caused by leukoaraiosis. *Frontiers in Neural Circuits*, *13*, 42.

Chen, P., Hartman, A. J., Priscilla Galarza, C., & DeLuca, J. (2012). Global processing training to improve visuospatial memory deficits after right-brain stroke. *Archives of Clinical Neuropsychology*, *27*, 891–905.

Cordonnier, C. (2011). Brain microbleeds: More evidence, but still a clinical dilemma. *Current Opinion in Neurology*, *24*, 69–74.

Damoiseaux, J. S., Rombouts, S. A., Barkhof, F., Scheltens, P., Stam, C. J., Smith, S. M., & Beckmann, C. F. (2006). Consistent resting-state networks across healthy subjects. *Proceedings of the National Academy of Sciences of the United States of America*, *103*, 13848–13853.

Debette, S., Schilling, S., Duperron, M. G., Larsson, S. C., & Markus, H. S. (2019). Clinical significance of magnetic resonance imaging markers of vascular brain injury: A systematic review and meta-analysis. *JAMA Neurology*, *76*, 81–94.

Ding, X., Ding, J., Hua, B., Xiong, X., Xiao, L., Peng, F., … Wang, Q. (2017). Abnormal cortical functional activity in patients with ischemic white matter lesions: A resting-state functional magnetic resonance imaging study. *Neuroscience Letters*, *644*, 10–17.

Fazekas, F., Chawluk, J. B., Alavi, A., Hurtig, H. I., & Zimmerman, R. A. (1987). MR signal abnormalities at 1.5 T in Alzheimer's dementia and normal aging. *AJR. American Journal of Roentgenology*, *149*, 351–356.

Friston, K. J., Williams, S., Howard, R., Frackowiak, R. S. J., & Turner, R. (1996). Movement-related effects in fMRI time-series. *Magnetic Resonance in Medicine*, *35*, 346–355.

Grau-Olivares, M., & Arboix, A. (2009). Mild cognitive impairment in stroke patients with ischemic cerebral small-vessel disease: A forerunner of vascular dementia? *Expert Review of Neurotherapeutics*, *9*, 1201–1217.

Greenberg, S. M., Vernooij, M. W., Cordonnier, C., Viswanathan, A., Al-Shahi Salman, R., Warach, S., … Breteler, M. M. (2009). Cerebral microbleeds: A guide to detection and interpretation. *Lancet Neurology*, *8*, 165–174.

Haller, S., Vernooij, M. W., Kuijer, J. P. A., Larsson, E. M., Jäger, H. R., & Barkhof, F. (2018). Cerebral microbleeds: Imaging and clinical significance. *Radiology*, *287*, 11–28.

He, X., Li, X., Fu, J., Xu, J., Liu, H., Zhang, P., … Qin, W. (2021). The morphometry of left cuneus mediating the genetic regulation on working memory. *Human Brain Mapping*, *42*, 3470–3480.

He, Y., Chen, Z., Gong, G., & Evans, A. (2009). Neuronal networks in Alzheimer's disease. *The Neuroscientist*, *15*, 333–350.

Heflin, L. H., Laluz, V., Jang, J., Ketelle, R., Miller, B. L., & Kramer, J. H. (2011). Let's inhibit our excitement: The relationships between Stroop, behavioral disinhibition, and the frontal lobes. *Neuropsychology*, *25*, 655–665.

Iadecola, C. (2017). The neurovascular unit coming of age: A journey through neurovascular coupling in health and disease. *Neuron*, *96*, 17–42.

Indovina, I., Conti, A., Lacquaniti, F., Staab, J. P., Passamonti, L., & Toschi, N. (2019). Reduced betweenness centrality of a sensory-motor vestibular network in subclinical agoraphobia. *Annual International Conference of the IEEE Engineering in Medicine and Biology Society*, *2019*, 4342–4345.

Jenkinson, M., Bannister, P., Brady, M., & Smith, S. (2002). Improved optimization for the robust and accurate linear registration and motion correction of brain images. *NeuroImage*, *17*, 825–841.

Kana, R. K., Uddin, L. Q., Kenet, T., Chugani, D., & Müller, R. A. (2014). Brain connectivity in autism. *Frontiers in Human Neuroscience*, *8*, 349.

Liao, X., Vasilakos, A. V., & He, Y. (2017). Small-world human brain networks: Perspectives and challenges. *Neuroscience and Biobehavioral Reviews*, *77*, 286–300.

Lisman, J., Buzsáki, G., Eichenbaum, H., Nadel, L., Ranganath, C., & Redish, A. D. (2017). Viewpoints: How the hippocampus contributes to memory, navigation and cognition. *Nature Neuroscience*, *20*, 1434–1447.

Liu, J. Y., Zhou, Y. J., Zhai, F. F., Han, F., Zhou, L. X., Ni, J., … Zhu, Y. C. (2020). Cerebral microbleeds are associated with loss of white matter integrity. *AJNR. American Journal of Neuroradiology*, *41*, 1397–1404.

Liu, R., Chen, H., Qin, R., Gu, Y., Chen, X., Zou, J., … Xu, Y. (2019). The altered reconfiguration pattern of brain modular architecture regulates cognitive function in cerebral small vessel disease. *Frontiers in Neurology*, *10*, 324.

Liu, R., Wu, W., Ye, Q., Gu, Y., Zou, J., Chen, X., … Wang, C. (2019). Distinctive and pervasive alterations of functional brain networks in cerebral small vessel disease with and without cognitive impairment. *Dementia and Geriatric Cognitive Disorders*, *47*, 55–67.

Low, A., Mak, E., Rowe, J. B., Markus, H. S., & O'Brien, J. T. (2019). Inflammation and cerebral small vessel disease: A systematic review. *Ageing Research Reviews*, *53*, 100916.

Lu, J., Li, D., Li, F., Zhou, A., Wang, F., Zuo, X., … Jia, J. (2011). Montreal cognitive assessment in detecting cognitive impairment in Chinese elderly individuals: A population-based study. *Journal of Geriatric Psychiatry and Neurology*, *24*, 184–190.

Mevel, K., Grassiot, B., Chételat, G., Defer, G., Desgranges, B., & Eustache, F. (2010). The default mode network: Cognitive role and pathological disturbances. *Revue Neurologique (Paris)*, *166*, 859–872.

Miotto, E. C., Balardin, J. B., Martin, M. D. G. M., Polanczyk, G. V., Savage, C. R., Miguel, E. C., & Batistuzzo, M. C. (2020). Effects of semantic categorization strategy training on episodic memory in children and adolescents. *PLoS One*, *15*, e0228866.

Miwa, K., Tanaka, M., Okazaki, S., Furukado, S., Sakaguchi, M., & Kitagawa, K. (2011). Relations of blood inflammatory marker levels with cerebral microbleeds. *Stroke*, *42*, 3202–3206.

Miwa, K., Tanaka, M., Okazaki, S., Yagita, Y., Sakaguchi, M., Mochizuki, H., & Kitagawa, K. (2014). Multiple or mixed cerebral microbleeds and dementia in patients with vascular risk factors. *Neurology*, *83*, 646–653.

Nannoni, S., Ohlmeier, L., Brown, R. B., Morris, R. G., MacKinnon, A. D., & Markus, H. S. (2021). Cognitive impact of cerebral microbleeds in patients with symptomatic small vessel disease. *International Journal of Stroke*. https://doi.org/10.1177/17474930211012837

O'Brien, J. T., Erkinjuntti, T., Reisberg, B., Roman, G., Sawada, T., Pantoni, L., … DeKosky, S. T. (2003). Vascular cognitive impairment. *Lancet Neurology*, *2*, 89–98.

Pantoni, L. (2010). Cerebral small vessel disease: From pathogenesis and clinical characteristics to therapeutic challenges. *Lancet Neurology*, *9*, 689–701.

Putcha, D., Brickhouse, M., Wolk, D. A., Dickerson, B. C., & Alzheimer's Disease Neuroimaging Initiative. (2019). Fractionating the Rey auditory verbal learning test: Distinct roles of large-scale cortical networks in prodromal Alzheimer's disease. *Neuropsychologia*, *129*, 83–92.

Qin, W., Xuan, Y., Liu, Y., Jiang, T., & Yu, C. (2015). Functional connectivity density in congenitally and late blind subjects. *Cerebral Cortex*, *25*, 2507–2516.

Qiu, Y. H., Huang, Z. H., Gao, Y. Y., Feng, S. J., Huang, B., Wang, W. Y., … Wang, L. J. (2021). Alterations in intrinsic functional networks in Parkinson's disease patients with depression: A resting-state functional magnetic resonance imaging study. *CNS Neuroscience & Therapeutics*, *27*, 289–298.

Raichle, M. E. (2015). The brain's default mode network. *Annual Review of Neuroscience*, *38*, 433–447.

Sala-Llonch, R., Palacios, E. M., Junqué, C., Bargalló, N., & Vendrell, P. (2015). Functional networks and structural connectivity of visuospatial and visuoperceptual working memory. *Frontiers in Human Neuroscience*, *9*, 340.

Samarasekera, N., Smith, C., & Al-Shahi Salman, R. (2012). The association between cerebral amyloid angiopathy and intracerebral haemorrhage: Systematic review and meta-analysis. *Journal of Neurology, Neurosurgery, and Psychiatry*, *83*, 275–281.

Scarpina, F., & Tagini, S. (2017). The Stroop color and word test. *Frontiers in Psychology*, *8*, 557.

Schaefer, A., Quinque, E. M., Kipping, J. A., Arélin, K., Roggenhofer, E., Frisch, S., … Schroeter, M. L. (2014). Early small vessel disease affects Frontoparietal and cerebellar hubs in close correlation with clinical symptoms—A resting-state fMRI study. *Journal of Cerebral Blood Flow and Metabolism*, *34*, 1091–1095.

Schreiber, S., Bueche, C. Z., Garz, C., & Braun, H. (2013). Blood brain barrier breakdown as the starting point of cerebral small vessel disease? - New insights from a rat model. *Experimental & Translational Stroke Medicine*, *5*, 4.

Schroeter, M. L., Stein, T., Maslowski, N., & Neumann, J. (2009). Neural correlates of Alzheimer's disease and mild cognitive impairment: A systematic and quantitative meta-analysis involving 1351 patients. *NeuroImage*, *47*, 1196–1206.

Schulz, M., Malherbe, C., Cheng, B., Thomalla, G., & Schlemm, E. (2021). Functional connectivity changes in cerebral small vessel disease - a systematic review of the resting-state MRI literature. *BMC Medicine*, *19*, 103.

Seghier, M. L. (2013). The angular gyrus: Multiple functions and multiple subdivisions. *The Neuroscientist*, *19*, 43–61.

Seo, S. W., Hwa Lee, B., Kim, E. J., Chin, J., Sun Cho, Y., Yoon, U., & Na, D. L. (2007). Clinical significance of microbleeds in subcortical vascular dementia. *Stroke*, *38*, 1949–1951.

Shackman, A. J., Salomons, T. V., Slagter, H. A., Fox, A. S., Winter, J. J., & Davidson, R. J. (2011). The integration of negative affect, pain and cognitive control in the cingulate cortex. *Nature Reviews. Neuroscience*, *12*, 154–167.

Sridharan, D., Levitin, D. J., & Menon, V. (2008). A critical role for the right fronto-insular cortex in switching between central-executive and default-mode networks. *Proceedings of the National Academy of Sciences of the United States of America*, *105*, 12569–12574.

Staffaroni, A. M., Brown, J. A., Casaletto, K. B., Elahi, F. M., Deng, J., Neuhaus, J., … Kramer, J. H. (2018). The longitudinal trajectory of default mode network connectivity in healthy older adults varies as a function of age and is associated with changes in episodic memory and processing speed. *The Journal of Neuroscience*, *38*, 2809–2817.

Sun, Y. W., Qin, L. D., Zhou, Y., Xu, Q., Qian, L. J., Tao, J., & Xu, J. R. (2011). Abnormal functional connectivity in patients with vascular cognitive impairment, no dementia: A resting-state functional magnetic resonance imaging study. *Behavioural Brain Research*, *223*, 388–394.

Telesford, Q. K., Joyce, K. E., Hayasaka, S., Burdette, J. H., & Laurienti, P. J. (2011). The ubiquity of small-world networks. *Brain Connectivity*, *1*, 367–375.

Thompson, C. S., & Hakim, A. M. (2009). Living beyond our physiological means: Small vessel disease of the brain is an expression of a systemic failure in arteriolar function: A unifying hypothesis. *Stroke*, *40*, e322–e330.

Tzourio-Mazoyer, N., Landeau, B., Papathanassiou, D., Crivello, F., Etard, O., Delcroix, N., … Joliot, M. (2002). Automated anatomical labeling of activations in SPM using a macroscopic anatomical parcellation of the MNI MRI single-subject brain. *NeuroImage*, *15*, 273–289.

Uddin, L. Q., Nomi, J. S., Hébert-Seropian, B., Ghaziri, J., & Boucher, O. (2017). Structure and function of the human insula. *Journal of Clinical Neurophysiology*, *34*, 300–306.

van den Heuvel, M. P., & Fornito, A. (2014). Brain networks in schizophrenia. *Neuropsychology Review*, *24*, 32–48.

van den Heuvel, M. P., & Sporns, O. (2013). Network hubs in the human brain. *Trends in Cognitive Sciences*, *17*, 683–696.

van Es, A. C., van der Grond, J., de Craen, A. J., Westendorp, R. G., Bollen, E. L., Blauw, G. J., … van Buchem, M. A. (2011). Cerebral microbleeds and cognitive functioning in the PROSPER study. *Neurology*, *77*, 1446–1452.

van Norden, A. G., van den Berg, H. A., de Laat, K. F., Gons, R. A., van Dijk, E. J., & de Leeuw, F. E. (2011). Frontal and temporal microbleeds are related to cognitive function: The Radboud University Nijmegen Diffusion Tensor and Magnetic Resonance Cohort (RUN DMC) study. *Stroke*, *42*, 3382–3386.

Wang, J., Chen, Y., Liang, H., Niedermayer, G., Chen, H., Li, Y., … Zhang, Y. (2019). The role of disturbed small-world networks in patients with white matter lesions and cognitive impairment revealed by resting state function magnetic resonance images (rs-fMRI). *Medical Science Monitor*, *25*, 341–356.

Wang, J., Li, T., Wang, N., Xian, J., & He, H. (2016). Graph theoretical analysis reveals the reorganization of the brain network pattern in primary open angle glaucoma patients. *European Radiology*, *26*, 3957–3967.

Wang, J., Wang, L., Zang, Y., Yang, H., Tang, H., Gong, Q., … He, Y. (2009). Parcellation-dependent small-world brain functional networks: A resting-state fMRI study. *Human Brain Mapping*, *30*, 1511–1523.

Wang, J., Wang, X., Xia, M., Liao, X., Evans, A., & He, Y. (2015). GRETNA: A graph theoretical network analysis toolbox for imaging connectomics. *Frontiers in Human Neuroscience*, *9*, 386.

Wang, J., Zuo, X., Dai, Z., Xia, M., Zhao, Z., Zhao, X., … He, Y. (2013). Disrupted functional brain connectome in individuals at risk for Alzheimer's disease. *Biological Psychiatry*, *73*, 472–481.

Wardlaw, J. M., Smith, C., & Dichgans, M. (2013). Mechanisms of sporadic cerebral small vessel disease: Insights from neuroimaging. *Lancet Neurology*, *12*, 483–497.

Wardlaw, J. M., Smith, E. E., Biessels, G. J., Cordonnier, C., Fazekas, F., Frayne, R., … Dichgans, M. (2013). Neuroimaging standards for research into small vessel disease and its contribution to ageing and neurodegeneration. *The Lancet Neurology*, *12*, 822–838.

Wei, M., Shi, J., Li, T., Ni, J., Zhang, X., Li, Y., … Tian, J. (2018). Diagnostic accuracy of the Chinese version of the trail-making test for screening cognitive impairment. *Journal of the American Geriatrics Society*, *66*, 92–99.

Weiner, K. S., & Zilles, K. (2016). The anatomical and functional specialization of the fusiform gyrus. *Neuropsychologia*, *83*, 48–62.

Wen, H., Liu, Y., Rekik, I., Wang, S., Chen, Z., Zhang, J., … He, H. (2018). Combining disrupted and discriminative topological properties of functional connectivity networks as neuroimaging biomarkers for accurate diagnosis of early Tourette syndrome children. *Molecular Neurobiology*, *55*, 3251–3269.

Wen, H., Liu, Y., Rekik, I., Wang, S., Zhang, J., Zhang, Y., … He, H. (2017). Disrupted topological organization of structural networks revealed by probabilistic diffusion tractography in Tourette syndrome children. *Human Brain Mapping*, *38*, 3988–4008.

Werring, D. J., Frazer, D. W., Coward, L. J., Losseff, N. A., Watt, H., Cipolotti, L., … Jäger, H. R. (2004). Cognitive dysfunction in patients with cerebral microbleeds on T2*-weighted gradient-echo MRI. *Brain*, *127*, 2265–2275.

Yan, C. G., Cheung, B., Kelly, C., Stan Colcombe, R., Craddock, C., Di Martino, A., … Milham, M. P. (2013). A comprehensive assessment of regional variation in the impact of head micromovements on functional connectomics. *NeuroImage*, *76*, 183–201.

Yi, L., Wang, J., Jia, L., Zhao, Z., Lu, J., Li, K., … Han, Y. (2012). Structural and functional changes in subcortical vascular mild cognitive impairment: A combined voxel-based morphometry and resting-state fMRI study. *PLoS One*, *7*, e44758.

Yi, L. Y., Liang, X., Liu, D. M., Sun, B., Ying, S., Yang, D. B., … Han, Y. (2015). Disrupted topological organization of resting-state functional brain network in subcortical vascular mild cognitive impairment. *CNS Neuroscience & Therapeutics*, *21*, 846–854.

Yong, H., Wang, J., Wang, L., Chen, Z. J., Chaogan, Y., Yang, H., … Yufeng, Z. (2009). Uncovering intrinsic modular Organization of Spontaneous Brain Activity in humans. *PLoS One*, *4*, e5226.

Young, V. G., Halliday, G. M., & Kril, J. J. (2008). Neuropathologic correlates of white matter hyperintensities. *Neurology*, *71*, 804–811.

Zhang, C. E., Wong, S. M., van de Haar, H. J., Staals, J., Jansen, J. F., Jeukens, C. R., … Backes, W. H. (2017). Blood-brain barrier leakage is more widespread in patients with cerebral small vessel disease. *Neurology*, *88*, 426–432.

Zhang, D., Liu, X., Chen, J., Liu, B., & Wang, J. (2015). Widespread increase of functional connectivity in Parkinson's disease with tremor: A resting-state FMRI study. *Frontiers in Aging Neuroscience*, *7*, 6.

Zhang, L., Ni, H., Yu, Z., Wang, J., Qin, J., Hou, F., … Alzheimer's Disease Neuroimaging Initiative. (2020). Investigation on the alteration of brain functional network and its role in the identification of mild cognitive impairment. *Frontiers in Neuroscience*, *14*, 1027.

Zhou, X., Hu, X., Zhang, C., Wang, H., Zhu, X., Xu, L., … Yu, Y. (2016). Aberrant functional connectivity and structural atrophy in subcortical vascular cognitive impairment: Relationship with cognitive impairments. *Frontiers in Aging Neuroscience*, *8*, 14.

Zhu, J., Zhuo, C., Liu, F., Qin, W., Xu, L., & Yu, C. (2016). Distinct disruptions of resting-state functional brain networks in familial and sporadic schizophrenia. *Scientific Reports*, *6*, 23577.

Zhu, Y., Lu, T., Xie, C., Wang, Q., Wang, Y., Cao, X., … Zhang, Z. (2020). Functional disorganization of small-world brain networks in patients with ischemic leukoaraiosis. *Frontiers in Aging Neuroscience*, *12*, 203.

SUPPORTING INFORMATION

Additional supporting information may be found in the online version of the article at the publisher's website.

How to cite this article: Xin, H., Wen, H., Feng, M., Gao, Y., Sui, C., Zhang, N., Liang, C., & Guo, L. (2022). Disrupted topological organization of resting-state functional brain networks in cerebral small vessel disease. *Human Brain Mapping*, *43*(8), 2607–2620. https://doi.org/10.1002/hbm.25808